



Hunting Young White Dwarfs at the Center of Planetary Nebulae

Javier A. Ahumada¹ , Walter A. Weidmann^{1,2}, Marcelo M. Miller Bertolami^{3,4} , and Leila Saker¹ 

¹ Observatorio Astronómico, Universidad Nacional de Córdoba, Laprida 854, 5000 Córdoba, Argentina; javier.ahumada@unc.edu.ar

² Consejo Nacional de Investigaciones Científicas y Técnicas, Argentina

³ Facultad de Ciencias Astronómicas y Geofísicas, Universidad Nacional de La Plata, Paseo del Bosque s/n, 1900 La Plata, Argentina

⁴ Instituto de Astrofísica La Plata, IALP, CONICET-UNLP, Paseo del Bosque s/n, 1900 La Plata, Argentina

Received 2018 August 25; revised 2019 July 31; accepted 2019 July 31; published 2019 September 16

Abstract

We present Gemini-South observations of nine faint and extended planetary nebulae (PNe). Using direct images taken with the spectrograph Gemini-South multi-object spectrograph (GMOS), we built the $(u' - g')$ versus $(g' - r')$ diagrams of the stars in the observed areas which allowed us to consider their geometrical positions and identify the probable central stars of the nebulae. Our stellar spectra of seven stars, also taken with GMOS, indicate that four (and probably two more) objects are white dwarfs of the DAO subtype. Moreover, the white dwarf status of the four stars is confirmed by the parameters T_{eff} and $\log g$ derived with the help of theoretical stellar spectra. Given this evidence, we propose that these hot stars are the central ionizing sources of the nebulae. With this work we hope to help improve the current scarce statistics on central white dwarfs in PNe.

Unified Astronomy Thesaurus concepts: Planetary nebulae nuclei (1250); Planetary nebulae (1249); White dwarf stars (1799); Subdwarf stars (2054)

1. Young White Dwarfs: The Ionizing Sources of Old Planetary Nebulae (PNe)

PNe are old, evolved objects, in which the slowly expanding, surrounding gas that an intermediate—or low-mass—star has lost during the asymptotic giant branch (AGB) phase, is ionized by the ultraviolet flux emanating from the central star. The nebula emits mainly in the ultraviolet, visible, and IR spectral regions. The central star of the nebula (CSPN) is essentially the hot stellar core, plus what is left of its initial envelope (Napiwotzki 1998; Dreizler 1999). While the morphologies of the PNe are amazingly diverse (Weidmann et al. 2016), the CSPNe also have a wide range of properties, with temperatures that range from $\approx 25,000$ to over $200,000$ K, luminosities from 10 to over $10,000 L_{\odot}$, and a display of astonishingly varied spectra. Although most CSPNe have hydrogen-rich atmospheres (Todt et al. 2006), there is, however, another class of central stars with atmospheres deficient in hydrogen. Some H-poor CSPNe have strong emission lines of highly ionized carbon, oxygen, and helium, and exhibit fast stellar winds—that produce broad emission lines—as well as high mass-loss rates (Weidmann et al. 2008). Finally, there is a small group of CSPNe showing rare spectral types e.g., O(He). As yet, the evolution of the CSPNe is not fully understood, in particular that of the H-deficient CSPNe. It is generally accepted that this evolutionary path begins with a late O-type star or a [WCL] star, depending on whether it is H-rich or H-poor, and ends up with a white dwarf (WD), of DA-type, or of DO-/DB-type, respectively (Napiwotzki 1998). A subclass of the DAs is that of the DAOs, whose spectra are characterized by broad Balmer lines together with a sharp He II feature at 4686 \AA (Wesemael et al. 1985). In the H-poor sequence, before the star becomes a WD, it is believed it goes through the PG 1159 stage. This is represented by stars showing a strong He II/C IV absorption trough around 4670 \AA and typical temperatures of $100,000$ K. The PG 1159 stars are key objects to fully understand the post-AGB evolution (Dreizler 1999). At present, although there are 3000 true and probable PNe known in the Milky Way, a stellar continuum has been detected in only 16% of them (Weidmann

& Gamen 2011). Less than 6% of these CSPNe are classified as WDs (i.e., 30 stars, of which 12 are DA-type, 14 are DAO, and 4 are DO) and, in most cases, they have been identified and classified from low-resolution spectra. Their study is increasingly difficult after the PN reaches its maximum brightness (i.e., approximately when nuclear fusion stops in the CSPNe), because the central star grows fainter while evolving down the white dwarf cooling track. The star finally turns undetectable like the PN, that by this time has become very dispersed.

This work is part of a current effort to unveil the properties of faint, so far unstudied CSPNe to gain knowledge on these stars and their evolution (Weidmann & Gamen 2011). In particular, we are interested in finding new WDs among CSPNe, because so few of them are currently known. Since the WDs are intrinsically faint objects, large telescopes are required for their detection and proper study. Here, we use photometric and spectroscopic data acquired with the 8.1 m Gemini-South Telescope, together with theoretical spectra and evolution models, to find and characterize the central white dwarfs of seven PNe: PN G019.7–10.7, PN G237.0+00.7, PN G276.2–06.6, PN G298.7–07.5, PN G302.1+00.3, PN G314.5–01.0, and PN G325.3–02.9. We also present the probable central stars of two additional nebulae, PN G328.5+06.0 and PN G344.9+03.0, for which we only possess Gemini photometry.

The structure of this paper is as follows: in Section 2, we justify our choice of the PNe and describe how we intend to find their central stars. In Section 3, we give an account of the photometric and spectroscopic observations performed with Gemini-South multi-object spectrograph (GMOS) at the Gemini-South Telescope. In Section 4, we explain the photometric analysis and the identification of the CSPNe. In Section 5, we present and discuss our spectroscopy of seven stars, obtain parameters T_{eff} and $\log g$ for four of them by employing TheoSSA synthetic spectra, and briefly examine some properties of hot subdwarfs that are, at the same time, CSPNe. Colors and distances for the CSPNe derived from the *Gaia* DR2 survey are discussed in Section 6. Using stellar

Table 1
Data of the Planetary Nebulae and of their Proposed Central Stars

Usual Name	PN				CSPN		
	PN G	Dimension (arcsec)	Morph ^a	$\log F_{\text{red}}^{\text{b}}$ (mW m^{-2})	α (h m s)	δ ($^{\circ}$ ' ")	r^{c} (mag)
MPA J1906–1634	019.7–10.7	242	B	–11.57	19 06 32.80	–16 34 00.3	18.8
PHR J0740–2055	237.0+00.7	240	Ra	–12.19	07 40 22.89	–20 55 54.5	18.1
PHR J0907–5722	276.2–06.6	241	Rsm	...	09 07 51.02	–57 22 52.9	18.7
PHR J1202–7000	298.7–07.5	317	Eas	–11.20	12 02 55.48	–70 00 56.8	19.7
RCW 69	302.1+00.3	300	B	–10.40	12 44 27.46	–62 31 18.9	19.1
PHR J1432–6138	314.5–01.0	180	Es	–10.90	14 32 09.65	–61 38 41.6	18.6
PHR J1553–5738	325.3–02.9	133	E	–11.45	15 53 09.87	–57 38 06.1	16.5
PHR J1533–4834	328.5+06.0	162	Rr	...	15 33 33.98	–48 34 24.7	18.6
BMP J1651–3930	344.9+03.0	315	Eas/Isa	...	16 51 41.27	–39 30 27.4	19.0

Notes.

^a Morphological classification, from the MASH catalogs (Parker et al. 2006, Miszalski et al. 2008).

^b Average red flux ($\text{H}\alpha + [\text{N II}]$), Frew et al. (2013).

^c Estimated value.

evolution model sequences, in Section 7, physical parameters of four CSPNe are computed. Summary and conclusions are in Section 8. In Appendix, we present finding charts for the nine stars.

2. Targets Selection

As suitable objects for searching new WDs as CSPNe, we selected nine PNe from the MASH catalogs⁵ (Parker et al. 2006; Miszalski et al. 2008). The PNe of our sample, listed in Table 1, have large angular sizes, symmetrical morphologies, and low surface brightness. We expect that objects with these properties are indeed old PNe, and therefore it is highly probable that their CSPNe are evolved objects, like white dwarfs. The MASH catalogs give the following comments on these nebulae:

PN G237.0+00.7: Very large, very faint, vaguely circular nebula; has strong $[\text{O III}]$ and no $\text{H}\beta$, $[\text{N II}] \approx \text{H}\alpha$; probable CSPNe position used for nebula center.

PN G276.2–06.6: Lovely faint, large, circular, evolved shell PN with enhanced NW edge; has $[\text{N II}] \approx 2 \times \text{H}\alpha$, $[\text{O III}] > \text{H}\beta$; has probable CSPNe.

PN G298.7–07.5: Very large, fractured oval nebula, possible evolved PN; also observed SA290603, MS060105; $[\text{N II}] > 10 \times \text{H}\alpha$, $[\text{O III}] > \text{H}\beta$; CSPNe at 12:02:55.5, –70:00:57.

PN G302.1+00.3: Bright, large, bipolar like structure, previously known as H II region RCW69; confirmed PN, has $[\text{N II}] > \text{H}\alpha$; also observed SA240603; was PHR1244–6230.

PN G314.5–01.0: Faint, extensive PN; confirmed by spectra. $[\text{N II}] \gtrsim 2.5 \times \text{H}\alpha$, $[\text{O III}] > \text{H}\beta$, CSPNe at 14:32:09.7, –61:38:41; previously NUN NeVe GN 14.28.3.01; possible IRAS source 14281–6127.

PN G325.3–02.9: Area of diffuse emission; $[\text{O III}] \approx 5 \times \text{H}\beta$, He II, $\text{H}\alpha$ only in red.

PN G328.5+06.0: Very faint ring nebula, $[\text{N II}] \approx 4 \times \text{H}\alpha$, $[\text{O III}] > \text{H}\beta$.

PN G344.9+03.0: PHR1626–5216 analog with striations.

Four probable CSPNe are reported by the MASH catalogs, found using their blue ($B_J - R_F < 0$) colors. We will use these identifications to check the results of our own strategy, which we describe next.

To identify the CSPNe among the stars present in the observed fields we use two criteria, namely, photometric and geometric. First, by performing photometry on the sky areas centered on the nebulae (Section 4), we build the color–color ($u' - g'$) versus ($g' - r'$) diagram. As shown by Girven et al. (2011), in this plane the white dwarfs lie along a sequence clearly differentiated from that of main-sequence stars. In Figure 2 (left panel) of Girven et al., the white-dwarf area is delimited with a line, and the knee of the upper main sequence appears at the bottom of the plot; for comparison, there is a calibrated main sequence in Figure 4 of Bilir et al. (2008). We then expect to find WD candidates, if there are any, in these parts of the diagrams. An objection to the use of our color–color diagrams could be raised, as they are built with instrumental magnitudes; this is because Band 4 nights, under which the photometric observations were performed (Section 3.1), are by definition non-photometric. This was done on purpose, since we are interested only in the general shapes of the sequences, and we expect that they do not change significantly in the instrumental system. Even the presence of thin clouds should only change the photometric zero-points and not the shapes of the sequences.

The second criterion of selection (geometric selection), complements the photometric: once a WD candidate is found in the color–color diagram, we check its position in the image. The star we are looking for should lie, in principle, at the geometrical center of the nebula—although there are known exceptions, such as, the central star of Sh2-174 (see Figure 5 of Napiwotzki (1998)). A nebula with symmetric, rounded morphology makes it easier to locate its center, helping us give more weight to this criterion.

3. Observations and Data Reduction

Our observations comprise, first, broad-band direct imaging of the nine nebulae, aimed at the identification of their ionizing stars; second, long-slit spectroscopy of such stars for their spectroscopic classification.

⁵ <https://heasarc.gsfc.nasa.gov/W3Browse/all/mashpncat.html>

Table 2
Some Remarks on the Observations

PN G	Mean FWHM ^a			Exposures ^b
	u'	g'	r'	
019.7–10.7	1.06	0.80	1.04	3×760
237.0+00.7	1.90	1.84	1.79	3×300
276.2–06.6	1.98	1.97	1.79	3×450
298.7–07.5	1.04	1.20	1.00	3×1200
302.1+00.3	1.52	1.58	1.36	3×925
314.5–01.0	1.70	1.12	1.20	3×650
325.3–02.9	1.38	0.88	1.50	3×1100
328.5+06.0	1.47	1.30	1.28	...
344.9+03.0	1.14	1.09	1.07	...

Notes.

^a For direct imaging, in arcseconds.

^b For spectroscopy data, in seconds.

3.1. Broad-band Optical Imaging

Direct images of the PNe of Table 1 were taken with the GMOS⁶ in its imaging mode, mounted on the 8.1 m Gemini-South Telescope at Cerro Pachón, Chile. The detector is an array of three 2048×4176 Hamamatsu chips arranged in a row. The array was configured in a 2×2 binning mode, which gave a scale of $0''.16/\text{pixel}$. The useful field covers a sky area of $5.5 \times 5.5 \text{ arcmin}^2$. The programs under which these data were obtained are GS-2016B-Q-92, GS-2017A-Q-90, and GS-2018A-Q-404 (PI: Weidmann), and were intended for Band 4 or “poor weather” nights, since the expected quality was considered sufficient for this part of the work (see Section 2).

The filters utilized were broad-band u' , g' , and r' , similar to those of the Sloan Digital Sky Survey (Fukugita et al. 1996). Per filter, several images were taken and combined after their processing with the Gemini IRAF package.⁷ The number of exposures and the integration times were, in all cases, the following: $4 \times 675 \text{ s}$ (u'), $8 \times 67 \text{ s}$ (g'), and $20 \times 60 \text{ s}$ (r'). With these exposure times it should be possible to observe an O-type star of magnitude $V = 19.5$ with a signal-to-noise ratio (S/N) of about 5. The quality of our final combined frames can be assessed by the mean FWHM of the stars in each band, which are shown in Table 2.

3.2. Spectroscopy Data

The data for spectroscopy were gathered under the Gemini programs GS-2017B-Q-80, GS-2018A-Q-301, GS-2019A-Q-304, and GS-2019A-Q-405 (PI: Weidmann). Seven out of the nine stars, found as described in Section 4, were observed with GMOS in its long-slit spectroscopic mode. Diffraction grating B600 was used with a slit width of $1''.0$, rendering a spectral resolution $R \approx 1400$ and a covered wavelength range that goes from 4000 to 7000 Å. The integration times for spectroscopy on source are given in Table 2.

Using IRAF⁸ tasks, the spectra were reduced following standard procedures: overscan and combined bias subtraction, dome flat-fields, and cosmic ray removal. The technique

⁶ <http://www.gemini.edu/sciops/instruments/gmos-0>

⁷ <http://www.gemini.edu/sciops/data-and-results/processing-software>

⁸ IRAF: the Image Reduction and Analysis Facility is distributed by the National Optical Astronomy Observatories, which are operated by the Association of Universities for Research in Astronomy, Inc., under cooperative agreement with the National Science Foundation.

employed to remove the nebular contribution is described in Weidmann et al. (2018). Finally, the three spectra per target were averaged.

4. Photometry

The photometry was carried out with DAOPHOT, in IRAF. Simple aperture photometry was performed on the u' , g' , and r' images, adopting small apertures of 1 FWHM of radius to achieve a good S/N relation; neither aperture correction nor standard stars were required. Figure 1 shows the nine instrumental ($u' - g'$) versus ($g' - r'$) diagrams. In all of the diagrams, the sequence of dwarfs is clearly seen and, in the zone of the white dwarfs (see Section 2), stars, marked by arrows, stand out. Since the locations of these stars indeed coincide with the centers of their respective nebulae, we propose that they are their ionizing sources. The J2000.0 coordinates of the nine stars are listed in Table 1 and the finding charts are shown in the Appendix.

Our positions are equal to the arcsecond for those CSPNe already indicated in the MASH catalogs. This confirms our results, and gives us confidence in the procedure we followed to do the detections. The coordinates of the remaining stars, moreover, are also very near to those of the PNe in the MASH catalogs; this is a further corroboration that our criterion of choosing symmetrical nebulae was essentially correct.

To estimate the Sloan magnitudes of the stars we made use of the AAVSO Photometric All-Sky Survey (APASS);⁹ this is conducted in five filters: Johnson B and V , and Sloan g' , r' , and i' , and is valid from about the 7th to the 17th magnitude. Starting with some stars in the field with available APASS r' magnitude, and comparing these magnitudes with our instrumental values, we estimated the r' magnitudes of the CSPNe listed in Table 1.

5. Spectral Classification

5.1. Main Features of the Spectra

Figure 2 shows the Gemini spectra of the stars found at the centers of PN G019.7–10.7, PN G237.0+00.7, PN G276.2–06.6, PN G298.7–07.5, PN G302.1+00.3, and PN G325.3–02.9. They display some evident features such as the Balmer series and a couple of He II lines, all of them fairly broadened. With this information, we are able to say that these stars belong to the H-rich group and are very hot.

Since Stark effect is the main cause of the broadening of absorption lines in spectra of hot WDs (Tremblay & Bergeron 2009), the value of the FWHM of spectral features could be a good criterion to help distinguish WDs from Population II O-type stars. In Table 3, we put together values of FWHM of several lines for our CSPNe, a sample of early O-type Population II stars and WDs from Weidmann et al. (2018), and early O subdwarfs from Drilling et al. (2013). It is evident that the FWHM of absorption lines of our stars are compatible with those of WDs. Moreover, the asymmetrical profiles shown by the Balmer lines could be caused by the presence of He II lines, which is typical of WDs spectra (McCook & Sion 1987). Given all this evidence, we classify the CSPNe of PN G019.7–10.7, PN G237.0+00.7, PN G276.2–06.6, and PN G325.3–02.9 as WDs of the DAO subtype.

⁹ <https://www.aavso.org/apass>

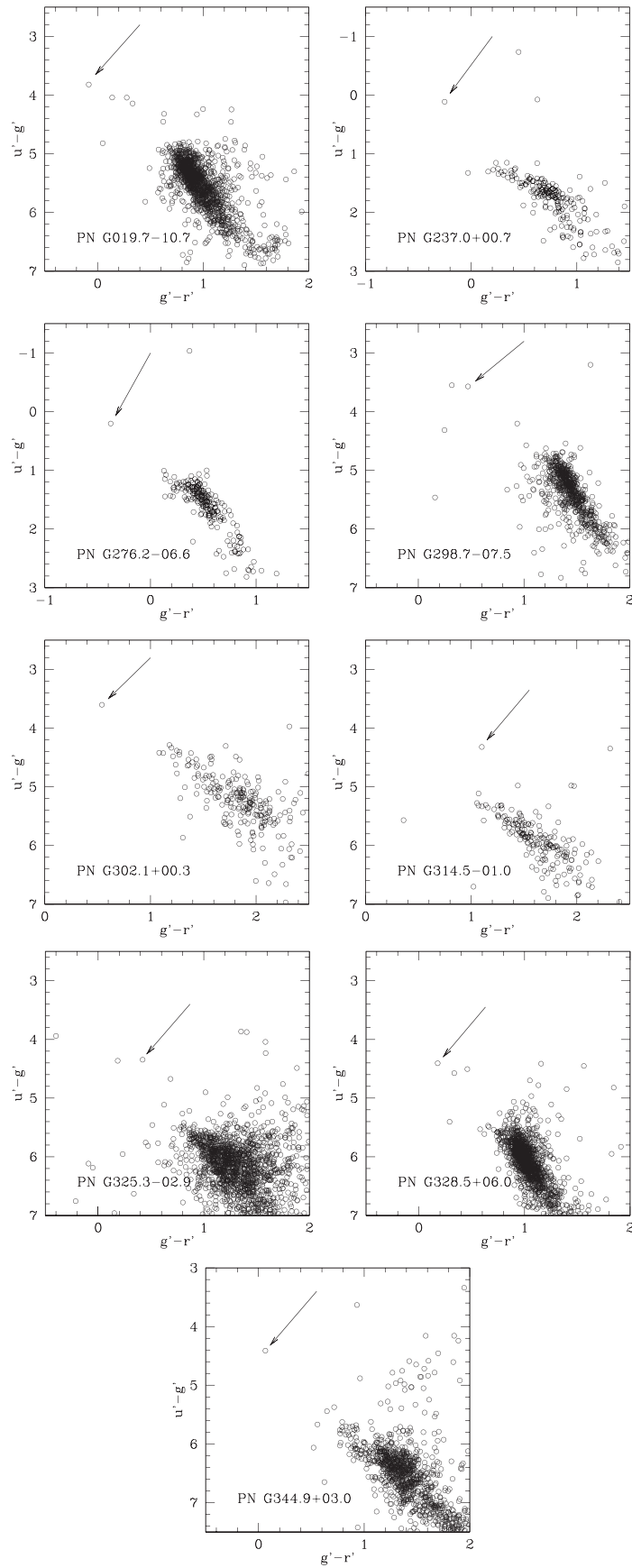


Figure 1. Instrumental $(u' - g')$ vs. $(g' - r')$ diagrams of the observed areas around the planetary nebulae under study. Each area is $5.5 \times 5.5 \text{ arcmin}^2$. The proposed central stars of the nebulae are marked by arrows.

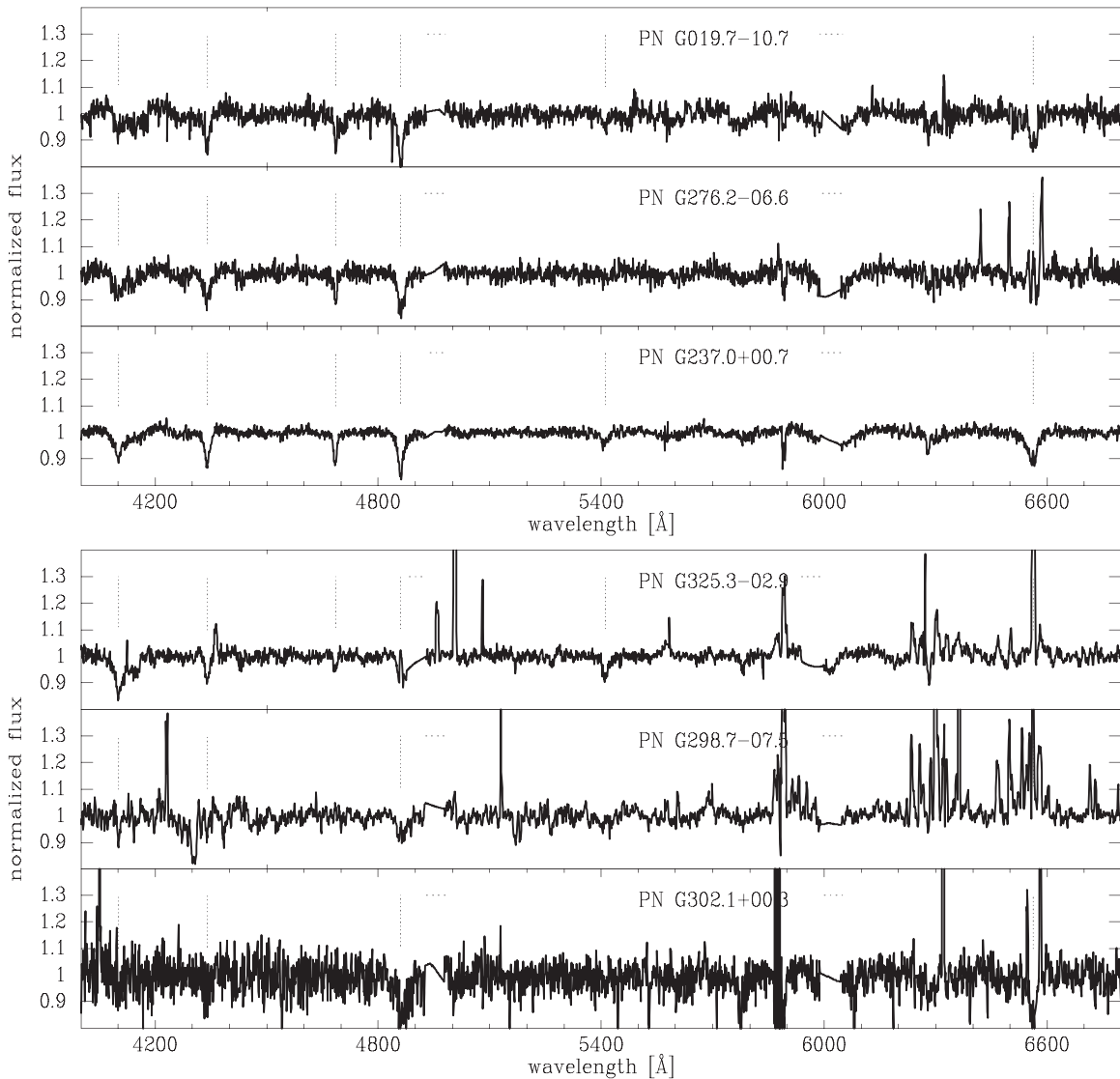


Figure 2. Normalized Gemini spectra of the central stars of PNe of our sample. The Balmer lines $H\alpha$, $H\beta$, $H\gamma$, and $H\delta$, and the He II lines at 4686 and 5412 Å are indicated with vertical dotted lines. The interstellar D-lines of Na I at 5890 and 5896 Å are not marked, but are clearly seen in the spectra. It is noteworthy that the absorption line at 6279 Å, a feature of unknown origin, also appears in the spectrum of the O(He)-type central star of the nebula K 1-27 (Rauch et al. 1996, 1998). The horizontal dotted lines mark the positions of the gaps separating the CCDs of the spectrograph.

However, we must point out that the spectra of PN G276.2–06.6 and PN G237.0+00.7 also display a combination of emission and absorption in $H\alpha$. This remarkable feature is particularly evident in the spectrum of PN G276.2–06.6. We believe that this emission is real, because the method used in Section 3.2 for subtracting the nebular contribution is especially efficient in large objects. We note that this characteristic is also present in the hot O-type subdwarf BD +28 4211 (Herbig 1999). Subdwarf O stars (sdOs) share properties with some CSPNe and DAO-type WDs (Heber 2016); there are few sdOs identified as CSPNe, and they are briefly discussed in Section 5.3.

The central star of RCW 69 was first pointed out by Frew et al. (2006). The authors did not obtain spectra of this star, and the physical parameters they give are highly uncertain. Even so, we agree with their identification, and classify this star as a possible WD.

We were not able to remove the nebular contribution in the spectrum of the central star of PN G325.3–02.9;

nevertheless, it shows evident, wide absorption lines of H and He II. The spectrum of the central star of PN G298.7–07.5 is very noisy and we could not detect any line of He II in it, so for now we classify the object as a possible WD. Finally, the spectrum of the central star of PN G314.5–01.0 has a moderate S/N but it does not display any features. Note that this does not necessarily rule out a WD classification; we categorize this star as “continuum” (Weidmann et al. 2018).

5.2. Effective Temperatures and Surface Gravities Derived with TheoSSA

To derive the stellar parameters T_{eff} and $\log g$ from our spectra, we employed the TheoSSA¹⁰ model, which is especially suitable for hot and compact stars like WDs. We followed the method given by Rauch et al. (2018) to properly

¹⁰ <http://astro.uni-tuebingen.de/~TMAW>

Table 3
Average FWHM (in Å) of Absorption Lines

Object	S/N ^a	FWHM (H γ)	FWHM (4686)	FWHM (H β)	N ^b
PN G019.7–10.7	46	14	10	20	...
PN G237.0+00.7	120	18	11	20	...
PN G276.2–06.6	60	25	9	23	...
PN G298.7–07.5	32	31	...
PN G302.1+00.3	18	37	...
PN G314.5–01.0	30
PN G325.3–02.9	65	14	10
O-type Population II stars ^c	...	9 \pm 2	6 \pm 2	9 \pm 2	12
sdO2–3 ^d	...	13 \pm 3	8 \pm 2	13 \pm 2	8
white dwarfs ^c	...	>13	>10	>17	3

Notes.

^a Ratios measured in the range 5050–5200 Å.

^b Number of objects used in the statistics.

^c Measurements on good-quality spectra of early O-type stars and WDs presented by Weidmann et al. (2018).

^d Measurements on spectra published by Drilling et al. (2013), considering only the hottest subtypes.

fit the line profiles. We considered stellar atmospheres composed only of H+He with solar abundances.

To address the problem reported by Napiwotzki & Rauch (1994), namely, that very different temperatures may be derived from the fits of different Balmer lines, we adopted the criterion of fitting the H δ line. The only exception was PN G019.7–10.7, whose H δ is very noisy; in this case, we used H γ instead.

Concerning the S/N ratio of our spectra, we want to remark that they were normalized and corrected by radial velocity. This procedure is essential to achieve a meaningful comparison with the TheoSSA model but, unfortunately, it further degrades the quality of the data. It is difficult to evaluate the uncertainties of the derived parameters, given the low quality of our spectra. Rough estimates of the uncertainties might be: $\Delta T_{\text{eff}} = 7000$ K and $\Delta \log g = 0.3$.

Our results for four CSPNe are displayed in Figure 3. The star of PN G325.3–02.9 deserves an extra comment. Its spectrum shows line profiles that are distorted, probably due to the normalization operation. The solution that we could obtain entails a couple of parameters that do not correspond to a CSPNe. Here we prefer to adopt uncertainties that at least double those given above.

Finally, we could not perform good fits for the objects PN G298.7–07.5 and PN G302.1+00.3, because their spectra are very noisy.

5.3. White Dwarfs or Hot Subdwarfs as CSPNe?

Although sdOs are relatively common objects, they appear scarcely related to PNe. Attempts to find nebulae around sdOs have had little success so far (Méndez et al. 1988; Kwitter et al. 1989), so much so that only five sdOs are currently known to be nuclei of PNe (Rauch et al. 2002; Aller et al. 2013, 2015). Of these stars perhaps the most relevant one is the sdO that ionizes the PN Ps 1, since this nebula appears physically associated to the globular cluster M15. There are four known PNe associated with globular clusters: Ps 1 in M15, IRAS 18333–2357 in M22, JaFu 1 in Pal 6,

and JaFu 2 in NGC 6441, with progenitor masses that range from 0.8 to 1.2 M_{\odot} (Jacoby et al. 2017). Thus far only for the first two nebulae it has been possible to assess the spectral type of their CSPNe, being sdO (Weidmann & Gamen 2011). This suggests that sdO is a final stage for stars of very low mass.

Since sdOs belong to the H-rich group of CSPNe (Drilling et al. 2013) like the DAs, how to distinguish one from another? According to Kepler et al. (2016), sdOs have $\log g < 6.5$ and DAs have $\log g > 7.0$. Consequently, and given the results of the current section, we can safely assume that our objects are indeed WDs.

6. Properties of the CSPNe Derived from *Gaia* DR2 Data

6.1. Magnitudes and Colors

The CSPNe under study were searched in the *Gaia* Data Release 2 Archive¹¹ (Gaia Collaboration et al. 2016, 2018) for information on parallaxes and colors, to help us characterize them better. The results of the search are in Table 4. It can be verified that *Gaia*'s G magnitudes and our APASS-estimated r' magnitudes (Table 1) are fairly similar. Although our sample is composed of early-type stars, some colors appear positive, especially those of PN G314.5–01.0, (whose colors, however, are consistent with the star's position in our color-color diagram in Figure 1). According to Andrae et al. (2018), indices $(G_{\text{BP}} - G)$ and $(G - G_{\text{RP}})$ are independent of the distance, unlike $(G_{\text{BP}} - G_{\text{RP}})$. Therefore, positive values of the said indices imply considerable reddenings. Assuming that these colors are correct, we can plot the $(G_{\text{BP}} - G)$ versus $(G - G_{\text{RP}})$ diagram (Figure 4). In this Figure, the majority of points follow roughly in a line, in which the most reddened star—although not the farthest one, see Section 6.2—is indeed that of PNG G314.5–01.0. For comparison, a similar plot for dereddened stars like Figure 4 of Andrae et al. (2018), indicates that our stars, that must be of approximately the same intrinsic color, should be grouped toward the lower left corner. In Figure 4, the central star of PN G302.1+00.3 seems to be the exception to the trend: perhaps its reddening is altered by the absorption originated in the nebula itself; in fact, its finding chart (Figure 6(e)) is the only one that shows clearly the nebula, at least through the filter r' .

6.2. Distances

The use of the estimator “parallax” (ϖ), given with an uncertainty σ_{ϖ} , to estimate the distance r has been thoroughly discussed by Luri et al. (2018) for the *Gaia* DR2 data. They show that the naive, direct interpretation of the distance as the simple inverse of the parallax is only accurate when the relative error $f = \sigma_{\varpi}/\varpi$ is at most 20%. Larger values of f require another, more careful approach, that should take advantage of the information that those imprecise (even negative, see Table 4) parallaxes may carry. Luri et al. (2018) recommend tackling this problem as an inference one, to be preferably handled with a full Bayesian approach. This method has been treated in depth by Bailer-Jones (2015): it involves estimating a “posterior probability” $P(r|\varpi, \sigma_{\varpi})$ over r , given the

¹¹ <https://gea.esac.esa.int/archive/>

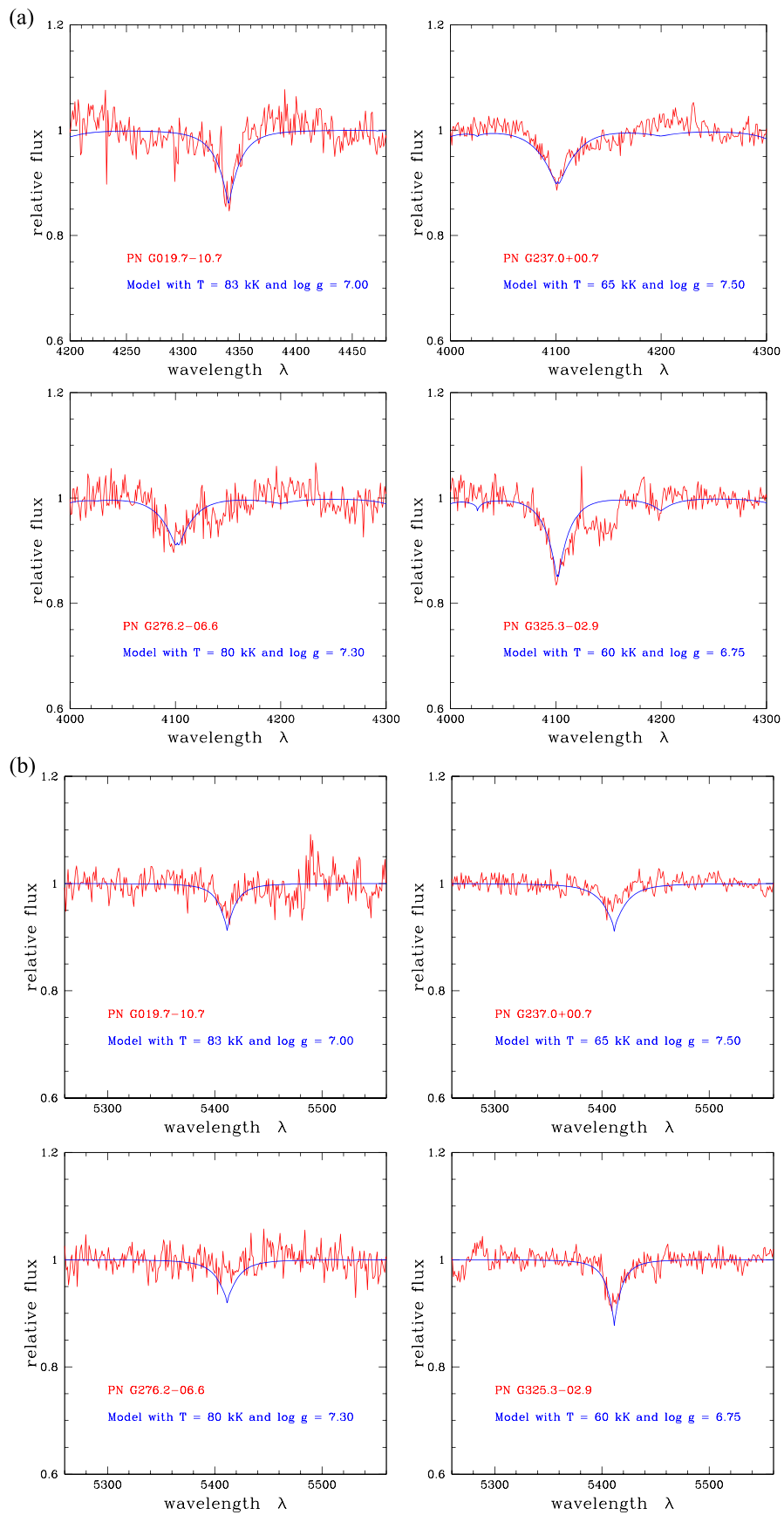


Figure 3. (a) Our line profiles compared with synthetic TheoSSA spectra. The line fit is H δ , except for PN G019.7-10.7, where H γ was used. The units of g are cm s^{-2} . (b) The He II (5411 Å) line is shown.

Table 4
Gaia Data and Derived Distances for the Central Stars of our Sample of PNe

PN G	<i>Gaia</i> DR2 Source Id.	Parallax (mas)	<i>G</i> (mag)	$G_{BP} - G_{RP}$ (mag)	$G_{BP} - G$ (mag)	$G - G_{RP}$ (mag)	Distance (pc)	90% CI (pc)
019.7–10.7	4088731114003376512	$+0.60 \pm 0.21$	18.452	−0.481	−0.235	−0.246	1826.80	[1324.88, 5622.94]
237.0+00.7	5715387335262528640	$+0.72 \pm 0.14$	18.128	−0.342	−0.183	−0.159	1433.15	[1139.40, 2547.80]
276.2–06.6	5303880196458455808	$+0.74 \pm 0.19$	18.762	−0.317	−0.265	−0.052	1453.84	[1104.38, 3805.05]
298.7–07.5	5855902039382099968	$−0.65 \pm 0.51$	19.973	−0.330	−0.218	−0.112	3903.66	[2176.32, 9692.69]
302.1+00.3	6055200341668022400	$+0.40 \pm 0.33$	19.407	+0.401	−0.403	+0.803	2603.64	[1563.92, 8112.72]
314.5–01.0	5878330972774696704	$+0.55 \pm 0.21$	18.528	+1.087	+0.304	+0.783	1996.02	[1412.34, 6271.82]
325.3–02.9	5835851723298840576	$−1.14 \pm 0.14$	16.690	+0.424	−0.057	+0.482
328.5+06.0	5986526735199975552	$+0.66 \pm 0.38$	18.698	+0.161	−0.248	+0.408	1981.30	[1225.92, 7477.57]
344.9+03.0	5970024611844351616	$+0.51 \pm 0.31$	19.027	+0.328	−0.052	+0.379	2260.15	[1431.83, 7583.31]

Table 5
 Properties of CSPNe Derived from Interpolation/extrapolation of the $Z = 0.01$ Stellar Evolution Models Presented by Miller Bertolami (2016)

PN G	$\log L_{CSPN}/L_{\odot}^a$	Age ^b (yr)	Age _{Min} ^c (yr)	Mass ^d (M_{\odot})	(M_{min}, M_{max}) ^e (M_{\odot})
019.7–10.7	$1.77^{+0.32}_{-0.31}$	2.5×10^5	1.4×10^5	0.508	($\lesssim 0.5, 0.538$)
237.0+00.7	$0.87^{+0.31}_{-0.28}$	6.9×10^5	3.1×10^5	0.543	($\lesssim 0.5, 0.628$)
276.2–06.6	$1.43^{+0.31}_{-0.30}$	2.9×10^5	0.7×10^5	0.532	($\lesssim 0.5, 0.596$)

Notes.

^a Interpolated CSPNe luminosity.

^b Interpolated post-AGB age.

^c Minimum post-AGB age consistent with the models within the error ellipse.

^d Interpolated mass.

^e Interpolated mass range consistent with the models within the error ellipse.

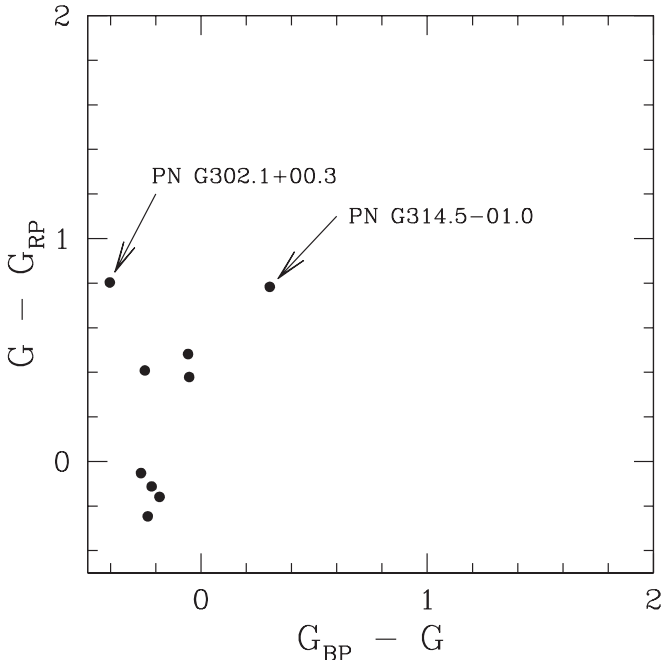


Figure 4. Color-color diagram in the *Gaia* photometric system for nine CSPNe.

observables (ϖ, σ_{ϖ}), as follows:

$$P(r|\varpi, \sigma_{\varpi}) = \frac{1}{Z} P(\varpi|r, \sigma_{\varpi}) P(r). \quad (1)$$

This is Bayes’ Theorem, in which $P(\varpi|r, \sigma_{\varpi})$ is the conditional probability of the observable parallax ϖ given r and σ_{ϖ} , $P(r)$ is

the prior probability (or simply “prior”), and Z is a normalization constant. The estimate of the distance is then the mode of the pdf $P(r|\varpi, \sigma_{\varpi})$. For the measurement model used in the *Gaia* data processing (Bailer-Jones 2015):

$$P(\varpi|r, \sigma_{\varpi}) = \frac{1}{\sqrt{2\pi}\sigma_{\varpi}} \exp\left[-\frac{1}{2\sigma_{\varpi}^2}\left(\varpi - \frac{1}{r}\right)^2\right]. \quad (2)$$

The prior expresses our knowledge of—or assumptions about—the distance, independent of ϖ . Bailer-Jones (2015) and Astraatmadja & Bailer-Jones (2016a, 2016b) discuss several priors, among them the “exponentially decreasing space density:”

$$P(r) = \begin{cases} \frac{1}{2L^3} r^2 e^{-r/L} & \text{if } r > 0, \\ 0 & \text{otherwise,} \end{cases} \quad (3)$$

with L a length scale. We choose it to estimate the distances of our CSPNe because it is simple, reasonable, and is available in the TOPCAT¹² software. The distances are in Table 4, given with 90% confidence intervals as recommended by Bailer-Jones (2015). We took $L = 1.35$ kpc, value suggested in the cited papers. The estimated distances appear to be reasonable, and are even consistent with the scale of relative apparent magnitudes, with the exception of PN G325.3–02.9. The *Gaia* parallax for this star is markedly negative, which results, through the adopted model, in an exceedingly large distance, in conflict with its brightness (Table 4) and reddening (Figure 4).

¹² <http://www.starlink.ac.uk/topcat/>

Table 6
Parameters for Planetary Nebulae in the Literature

Usual Name	PN G	Sp. Type	T_{eff} (10^3 K)	$\log g$ (cm s^{-2})	References
Sh 2-68	030.6+06.2	hybrid	84	7.24	Gianninas et al. (2010)
NGC 7293	036.1–57.1	DAO	90	6.90	Méndez et al. (1992)
NGC 6853	060.8–03.6	DAO	87	7.36	Gianninas et al. (2010)
NGC 6720	063.1+13.9	hgO(H)	101	6.90	Guerrero & De Marco (2013)
A66 61	077.6+14.7	DAO	88	7.10	Napiwotzki (1999)
Sh 2-188	128.0–04.1	DAO	87	7.41	Gianninas et al. (2010)
NGC 3587	148.4+57.0	DAO	94	6.90	Guerrero & De Marco (2013)
HDW 3	149.4–09.2	DAO	91	7.32	Gianninas et al. (2010)
PuWe 1	158.9+17.8	DAO	94	7.10	Guerrero & De Marco (2013)
A66 7	215.5–30.8	DAO	99	7.00	Guerrero & De Marco (2013)
EGB 6	221.5+46.3	DAOZ	100	7.00	Gathier & Pottasch (1988)
A66 35	303.6+40.0	DAO	80	7.20	Ziegler et al. (2012)

Note. This table includes the 30% of known WDs.

7. Comparison with Stellar Evolution Models

For the four CSPNe for which we have values of T_{eff} and $\log g$, it is now possible to derive other stellar properties using stellar evolution model sequences. In Table 5 we show the values of luminosity, age, and mass derived for our CSPNe by interpolating/extrapolating in T_{eff} and $\log g$ within the $Z = 0.01$ post-AGB sequences of Miller Bertolami (2016). The comparison of the parameters of our CSPNe with the interpolated tracks is shown in the lower panel of Figure 5. It is clear from this figure that, with the current values of T_{eff} and $\log g$, the central star of PN G325.3–02.9 falls outside the expected range for post-AGB stars, pointing to a very low mass object, with $M_{\text{CSPN}} \lesssim 0.5 M_{\odot}$. If this is the case, then the central star of PN G325.3–02.9 could be the descendent of a former hot subdwarf star that avoided the AGB phase, which implies that the surrounding nebula cannot be a bona fide PN. Due to the relatively low temperatures and high gravities derived from our spectra, the four CSPNe are consistent with low masses and large post-AGB ages. In particular, the latter are well beyond the expected lifetimes of PNe, rising questions about either the actual status of the PNe, or the accuracy of the parameters derived from our spectroscopy. Concerning the first point, perhaps one can legitimately wonder if all the objects under study are bona fide PNe: after all, all of them have received little attention so far; perhaps the ionized gas is interstellar material and not the star’s ejection, and the star is not a post-AGB star at all, or perhaps the central star has suffered more than one mass ejection, making the object appear like a younger PN, masking its true age. It is known, for example, that the presence and evolution of a binary at the center of a PN may affect the nebular morphology (Figure 1, Boffin et al. 2012), and even produce double shells (A66 65, Huckvale et al. 2013). About the second point, we note that our spectra are not of high quality, and that the comparisons with the TheoSSA models are based on the fitting of just *one* line, assuming a certain chemical composition. For these reasons, we can admit that the values of T_{eff} and $\log g$ we used are debatable. However, when we search the literature for estimated T_{eff} and $\log g$ for other PNe, it becomes apparent that our parameters are not so out of place among them. In Table 6, where we put together data for thirteen CSPNe from different sources, our objects fall in, or near, the ranges of parameters listed.

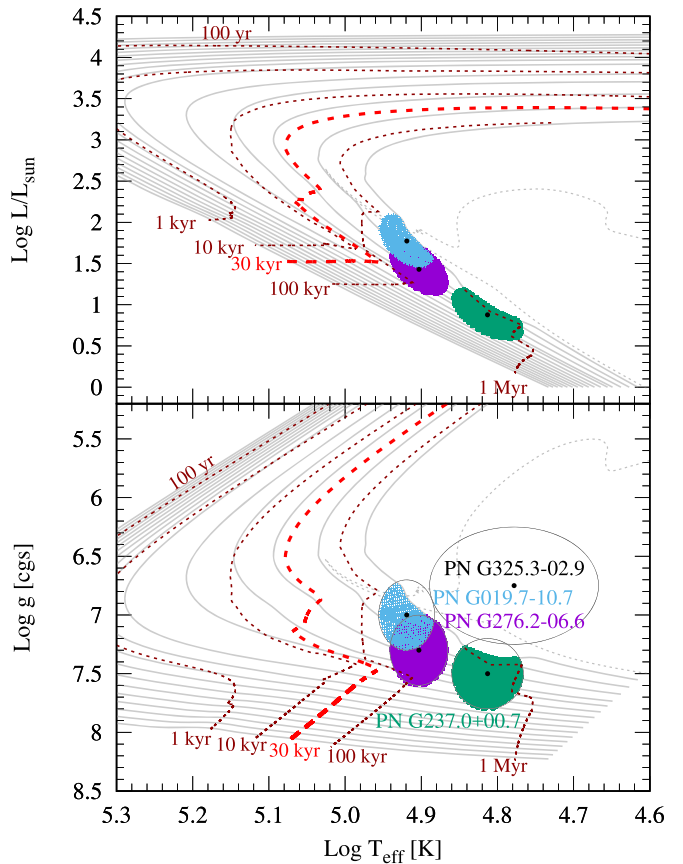


Figure 5. Bottom panel: Kiel diagram showing the location of the CSPNe with derived $\log T_{\text{eff}}$ and $\log g$ values, together with tracks interpolated/extrapolated from the $Z = 0.01$ post-AGB evolutionary sequences of Miller Bertolami (2016). From right to left, tracks are shown as solid lines for masses from $0.50 M_{\odot}$ to $0.80 M_{\odot}$, with a step of $0.02 M_{\odot}$. The dashed gray line at low temperatures and gravities corresponds to a post hot-subdwarf model ($M = 0.4754 M_{\odot}$) that avoided the AGB phase. Upper panel: HR diagram showing the luminosities of the central stars derived from interpolation/extrapolation from stellar evolution models.

8. Summary and Conclusions

We have presented a method for identifying white dwarfs as nuclei of PNe. The first results of this procedure have been very satisfactory. Using Gemini-GMOS images and spectra, we have

Table 7
Summary of Parameters for the CSPNe Found in this Work

PN G	T_{eff} (10^3 K)	$\log g$ (cm s^{-2})	Sp. Type	G (mag)	$G_{\text{BP}} - G_{\text{RP}}$ (mag)	Distance (kpc)
019.7–10.7	83	7.00	DAO	18.452	−0.481	1.83
237.0+00.7	65	7.50	DAO	18.128	−0.342	1.43
276.2–06.6	80	7.30	DAO	18.762	−0.317	1.45
298.7–07.5	WD?	19.973	−0.330	3.90
302.1+00.3	WD?	19.407	+0.401	2.60
314.5–01.0	cont.	18.528	+1.087	2.00
325.3–02.9	60	6.75	DAO	16.690	+0.424	...
328.5+06.0	18.698	+0.161	1.98
344.9+03.0	19.027	+0.328	2.26

been able to find and characterize the ionizing sources of seven old nebulae, PN G019.7–10.7, PN G237.0+00.7, PN G276.2–06.6, PN G298.7–07.5, PN G302.1+00.3, PN G314.5–01.0, and PN G325.3–02.9. Based on the analysis of our spectra and the modeling of the stellar atmospheres, we conclude that four of these stars are white dwarfs of type DAO, that another two are also likely WDs, and that we cannot discard the last star as a WD as well. Another two possible CSPNe, those of PN G328.5+06.0 and PN G344.9+03.0, have also been identified based on photometric data. Parameters for each CSPNe, including *Gaia*-DR2 distances and colors, have been collected in Table 7.

These objects have colors ($u' - g'$) and ($g' - r'$) that are compatible with those of WDs, and they are at the geometric center of PNe of large angular sizes and low surface brightness (i.e., old PNe). The spectra allowed us to classify the stars as WDs. The FWHM of absorption lines is compatible with those of WD's spectra. *Gaia* colors (allowing for reddening) indicate that they are blue objects. The TheoSSA atmosphere models permitted us to derive T_{eff} and $\log g$, obtaining values that are typical of white dwarfs and not of hot subdwarfs. We conclude, without doubt, that we have identified at least six white dwarfs—four of them of the DAO subtype—as the ionizing sources of PNe.

We are currently applying this procedure to a number of similar PNe observed with the same telescope and instrument. Our goal is to extend the sample of known WDs as CSPNe by 50%, i.e., to identify and classify at least fifteen new stars of this kind.

We believe that it is important to increase the known number of WDs that are, at the same time, CSPNe, as well as to improve their spectral classification. This will result in a refinement of the evolutionary models for the progenitors of the PNe and, consequently, in a better understanding of these fascinating objects.

Based on observations obtained at the Gemini Observatory and processed using the Gemini IRAF package. The Gemini

Observatory is operated by the Association of Universities for Research in Astronomy, Inc., under a cooperative agreement with the NSF on behalf of the Gemini partnership: the National Science Foundation (United States), the National Research Council (Canada), CONICYT (Chile), Ministerio de Ciencia, Tecnología e Innovación Productiva (Argentina), and Ministério da Ciência, Tecnologia e Inovação (Brazil). This research was made possible through the use of the AAVSO Photometric All-Sky Survey (APASS), funded by the Robert Martin Ayers Sciences Fund. W. W. would like to thank S. O. Kepler Oliveira and R. H. Méndez for their useful comments. Part of this research was supported by grant SeCyT UNC project No. 33820180100080CB. This work has made use of data from the European Space Agency (ESA) mission *Gaia* (<https://www.cosmos.esa.int/gaia>), processed by the *Gaia* Data Processing and Analysis Consortium (DPAC, <https://www.cosmos.esa.int/web/gaia/dpac/consortium>). Funding for the DPAC has been provided by national institutions, in particular the institutions participating in the *Gaia* Multilateral Agreement. The TMAW tool (<http://astro.uni-tuebingen.de/~TMAW>) used for this paper was constructed as part of the activities of the German Astrophysical Virtual Observatory. This research has made use of NASA's Astrophysics Data System and the SIMBAD database, operated at CDS, Strasbourg, France. Finally, we would like to thank the anonymous reviewer, whose comments and suggestions greatly helped to improve this paper.

Facility: GEMINI:South(GMOS).

Software: Aladin (Bonnarel et al. 2000), IRAF (Tody 1993), TMAW (Rauch et al. 2018), TOPCAT (Taylor 2005).

Appendix Finding Charts For the CSPNe

Figures 6 and 7 show the finding charts for the stars identified in this work, and whose coordinates are listed in Table 1.

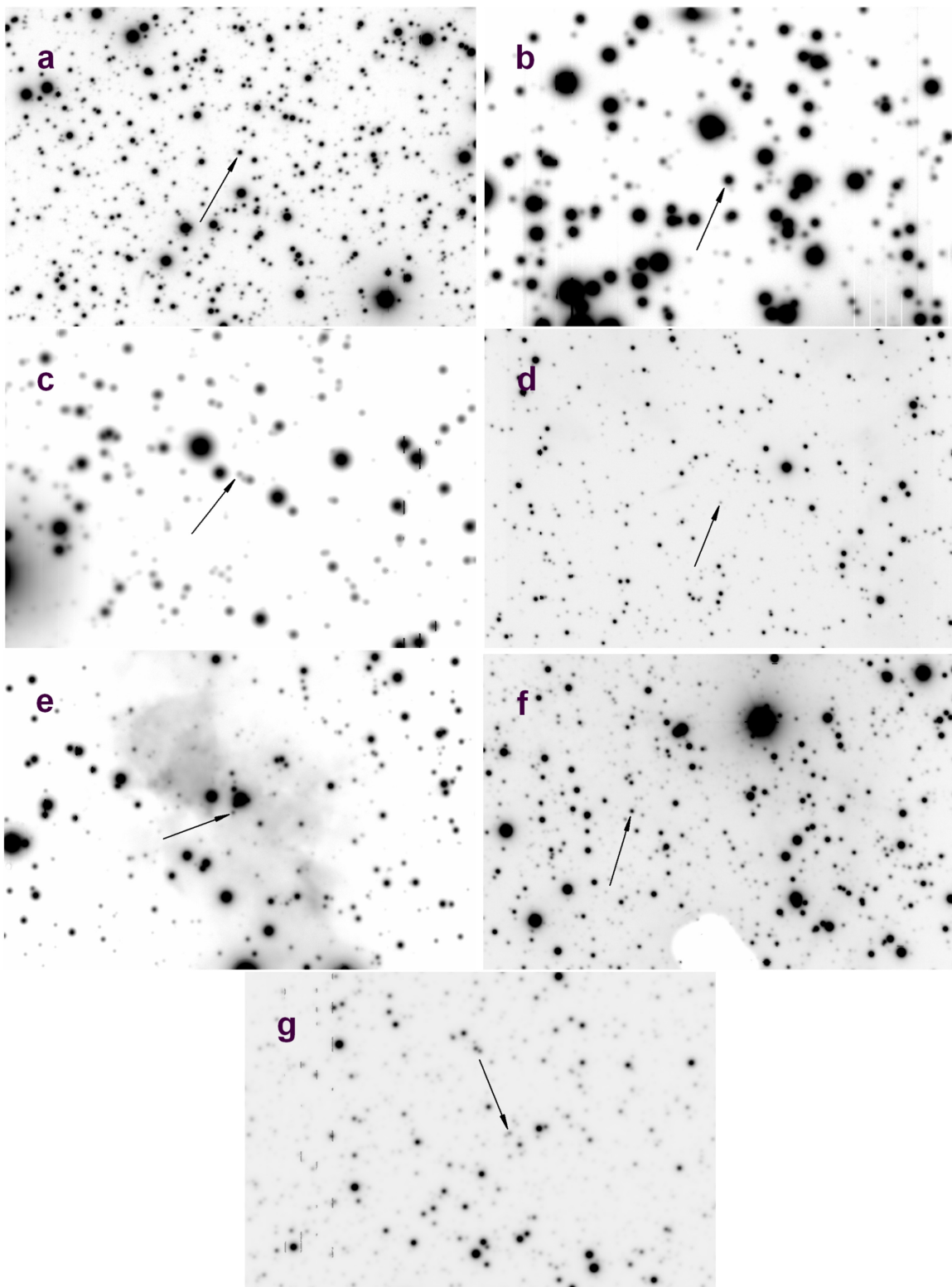


Figure 6. Finding charts, adapted from our r' images, for the proposed central stars of the planetary nebulae PN G019.7–10.7 (a), 237.0+00.7 (b), 276.2–06.6 (c), 298.7–07.5 (d), 302.1+00.3 (e), 314.5–01.0 (f), and 325.3–02.9 (g). The stars are marked by arrows and their coordinates are in Table 1. All charts cover areas of $3' \times 2'$. North is up and east is to the left.

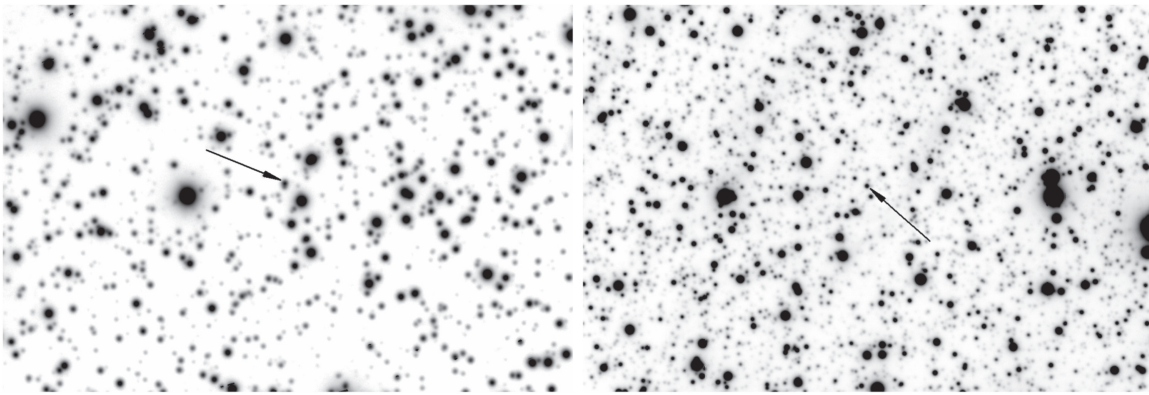




Figure 7. The same as in Figure 6, for PN G328.5+06.0 (left) and PN G344.9+03.0 (right).

ORCID iDs

Javier A. Ahumada  <https://orcid.org/0000-0002-7091-5025>

Marcelo M. Miller Bertolami  <https://orcid.org/0000-0001-8031-1957>

Leila Saker  <https://orcid.org/0000-0002-2227-5799>

References

- Aller, A., Miranda, L. F., Olguín, L., et al. 2015, *MNRAS*, 446, 317
- Aller, A., Miranda, L. F., Ulla, A., et al. 2013, *A&A*, 552, A25
- Andrae, R., Fouesneau, M., Creevey, O., et al. 2018, *A&A*, 616, A8
- Astraatmadja, T. L., & Bailer-Jones, C. A. L. 2016a, *ApJ*, 832, 137
- Astraatmadja, T. L., & Bailer-Jones, C. A. L. 2016b, *ApJ*, 833, 119
- Bailer-Jones, C. A. L. 2015, *PASP*, 127, 994
- Bilir, S., Ak, S., Karaali, S., et al. 2008, *MNRAS*, 384, 1178
- Boffin, H. M. J., Miszalski, B., Rauch, T., et al. 2012, *Sci*, 338, 773
- Bonnarel, F., Fernique, P., Bienaymé, O., et al. 2000, *A&AS*, 143, 33
- Dreizler, S. 1999, *RvMA*, 12, 255
- Drilling, J. S., Jeffery, C. S., Heber, U., Moehler, S., & Napiwotzki, R. 2013, *A&A*, 551, A31
- Frew, D. J., Bojičić, I. S., & Parker, Q. A. 2013, *MNRAS*, 431, 2
- Frew, D. J., Parker, Q. A., & Russeil, D. 2006, *MNRAS*, 372, 1081
- Fukugita, M., Ichikawa, T., Gunn, J. E., et al. 1996, *AJ*, 111, 1748
- Gaia Collaboration, Brown, A. G. A., Vallenari, A., et al. 2018, *A&A*, 616, A1
- Gaia Collaboration, Prusti, T., de Bruijne, J. H. J., et al. 2016, *A&A*, 595, A1
- Gathier, R., & Pottasch, S. R. 1988, *A&A*, 197, 266
- Gianninas, A., Bergeron, P., Dupuis, J., & Ruiz, M. T. 2010, *ApJ*, 720, 581
- Girven, J., Gänsicke, B. T., Steeghs, D., & Koester, D. 2011, *MNRAS*, 417, 1210
- Guerrero, M. A., & De Marco, O. 2013, *A&A*, 553, A126
- Heber, U. 2016, *PASP*, 128, 082001
- Herbig, G. H. 1999, *PASP*, 111, 1144
- Huckvale, L., Prouse, B., Jones, D., et al. 2013, *MNRAS*, 434, 1505
- Jacoby, G. H., De Marco, O., Davies, J., et al. 2017, *ApJ*, 836, 93
- Kepler, S. O., Pelisoli, I., Koester, D., et al. 2016, *MNRAS*, 455, 3413
- Kwitter, K. B., Massey, P., Congdon, C. W., & Pasachoff, J. M. 1989, *AJ*, 97, 1423
- Luri, X., Brown, A. G. A., Sarro, L. M., et al. 2018, *A&A*, 616, A9
- McCook, G. P., & Sion, E. M. 1987, *ApJS*, 65, 603
- Méndez, R. H., Gathier, R., Simon, K. P., & Kwitter, K. B. 1988, *A&A*, 198, 287
- Méndez, R. H., Kudritzki, R. P., & Herrero, A. 1992, *A&A*, 260, 329
- Miller Bertolami, M. M. 2016, *A&A*, 588, A25
- Miszalski, B., Parker, Q. A., Acker, A., et al. 2008, *MNRAS*, 384, 525
- Napiwotzki, R. 1998, *RvMA*, 11, 3
- Napiwotzki, R. 1999, *A&A*, 350, 101
- Napiwotzki, R., & Rauch, T. 1994, *A&A*, 285, 603
- Parker, Q. A., Acker, A., Frew, D. J., et al. 2006, *MNRAS*, 373, 79
- Rauch, T., Demleitner, M., Hoyer, D., & Werner, K. 2018, *MNRAS*, 475, 3896
- Rauch, T., Dreizler, S., & Wolff, B. 1998, *A&A*, 338, 651
- Rauch, T., Heber, U., & Werner, K. 2002, *A&A*, 381, 1007
- Rauch, T., Koeppe, J., & Werner, K. 1996, *A&A*, 310, 613
- Taylor, M. B. 2005, in *ASP Conf. Ser. 347, Astronomical Data Analysis Software and Systems XIV*, ed. P. Shopbell, M. Britton, & R. Ebert (San Francisco, CA: ASP), 29
- Todt, H., Gräfener, G., & Hamann, W.-R. 2006, in *IAU Symp. 234, Planetary Nebulae in our Galaxy and Beyond*, ed. M. J. Barlow & R. H. Méndez (Cambridge: Cambridge University Press), 127
- Tody, D. 1993, in *ASP Conf. Ser. 52, Astronomical Data Analysis Software and Systems II*, ed. R. J. Hanisch, R. J. V. Brissenden, & J. Barnes (San Francisco, CA: ASP), 173
- Tremblay, P.-E., & Bergeron, P. 2009, *ApJ*, 696, 1755
- Weidmann, W., Gamen, R., Mast, D., et al. 2018, *A&A*, 614, A135
- Weidmann, W. A., & Gamen, R. 2011, *A&A*, 526, A6
- Weidmann, W. A., Gamen, R., Díaz, R. J., & Niemela, V. S. 2008, *A&A*, 488, 245
- Weidmann, W. A., Schmidt, E. O., Vena Valdarenas, R. R., et al. 2016, *A&A*, 592, A103
- Wesemael, F., Green, R. F., & Liebert, J. 1985, *ApJS*, 58, 379
- Ziegler, M., Rauch, T., Werner, K., Köppen, J., & Kruk, J. W. 2012, *A&A*, 548, A109